

# Optimization of Factors Affecting the Performance of a Fluidized Bed Dryer

Soner Çelen\* and Sultan Pektaş

Tekirdag Namik Kemal University, Corlu Faculty of Engineering, Department of Mechanical Engineering, 59830, Tekirdağ, Turkey

\*Author for correspondence: Email: scelen@nku.edu.tr; Tel: +90 282 250 2366

Received: September 12, 2022 / Revised: October 04, 2023 / Accepted: October 13, 2023

**This study investigated the theoretical, analytical, and experimental effects of parameters such as bed height, air velocity, and air temperature on drying using a fluidized bed dryer. The objective was to examine how these parameters influence the drying process of salt products in a pilot fluidized bed dryer and establish the foundation for the development of a future full-scale machine. Salt products with an initial moisture content of 3% were used in all experimental trials. The pressure drop was determined by calculating the minimum fluidization rate, Archimedes and Reynolds number. The calculated values were compared with the analyses conducted using the Multiphase Flow with Interphase eXchanges (MFIx) program and the tests performed on the pilot-scale static fluidized bed dryer equipment to verify the accuracy. Upon comparing the parameters in fluidized bed drying, it was concluded that the increase in air velocity had a more significant impact on the pressure drop than what was predicted in the theoretical calculations. Nevertheless, it was noted that the analysis was significantly impacted by the height of the bed.**

**Keywords:** fluidized bed dryer, salt drying, fluidization rate, pressure drop

## INTRODUCTION

Salt is a mineral that is generally used as a condiment and food preservative. In ancient times, it played an important role in the historical development of civilizations (Elias et al. 2019). Salt is used directly or indirectly in agriculture, animal husbandry, medicine, traffic, and industry, particularly as food (Güngörmez 2015). The production of salt typically involves the extraction, purification, and drying of seawater. In one of the production methods, crystalline sea salt is dried, pulverized, packaged, and distributed to the market. The drying process is essential for achieving the desired properties of salt, ensuring its longevity in storage (Demirkol et al. 2018).

In the case of lake salt, similar to other sources of salt production, it undergoes a series of processes including pooling, settling, collection, blending, and transportation to obtain raw salt. Salt enterprises employ various techniques to refine raw salt based on their establishment's structure, involving processes such as washing, evaporation, grinding, centrifugation, and drying, among others (Ersöz and Doğan 2010; Pektaş 2022).

Drying is a crucial process with widespread industrial applications, spanning sectors such as food, agriculture, mining, and manufacturing (Jafari and Farahbod 2017; Moralar and Çelen 2022). Drying is the process of removing water from a substance by using a heat source to provide sufficient energy for evaporation to take place. Drying is employed in various industries including food, medicine, chemistry, mining, and recycling (Kepceoğlu et al. 2020).

The drying process offers several advantages such as reducing the risk of fermentation, increasing storage capacity by removing water molecules, enabling the recycling of domestic and industrial waste, and reducing shipping and packaging costs. While drying methods may vary depending on the product, some commonly used dryer types include rotary dryers, belt dryers, vacuum dryers, spray dryers, and fluid bed dryers (Pektaş 2022).

Fluid bed dryers are process systems in which the drying process is carried out by fluidizing a moist product and allowing it to remain suspended in the air for a specific period of time. Air is supplied from the bottom to keep the product in a suspended state, thereby increasing the contact surface area with the air and

maximizing the drying efficiency. The design of a fluidized bed dryer involves various parameters that determine the machine's dimensions such as the initial moisture content of the product, desired final moisture content, product capacity, final product temperature, particle size, bed height, drying air velocity, drying temperature, particle entrainment, saltation, and terminal velocity.

Many studies have been carried out using fluid bed dryers. Calban (2006) studied the effects of bed height and the initial moisture concentration of the coal on drying behavior. Assari et al. (2007) developed a mathematical model for batch drying based on the Eulerian "two-fluid models". An agitated fluid bed dryer (AFBD) of pilot-scale capacity was designed to study the effect of the type of agitator and its speed, gas velocity, and inlet temperature and feed loading on the hydrodynamic performance of the AFBD by Bait et al. (2011). Hamzehei (2011) investigated the application of computational fluid dynamic (CFD) techniques on the hydrodynamics of a two-dimensional nonreactive gas-solid fluidized bed dryer. The effect of fluidizing gas velocity on the heat transfer coefficient in the immersed horizontal tube is discussed by Kamble et al. (2014). Jalali et al. (2018) also presented a computational model for the riser section of a lab-scale circulating fluidized bed operated at ambient temperature. In Mahmoodi et al.'s (2019) study, CFD and the discrete element method (DEM) were used in conjunction with the Eulerian-Lagrangian method to simulate a pseudo-two-dimensional spouted bed comprising coarse 6-mm particles. Pektaş (2022) investigated the optimization of factors affecting the performance of a fluidized bed dryer, while Godin et al. (2023) presented a study on particle entrainment from a fluidized bed of coke particles operated at high gas velocity and using a large column to avoid slugging.

This study's objective was to evaluate the precision of the calculation methods by investigating the parameters of drying air velocity, air temperature, and bed height prior to the design of a fluid bed dryer. These calculated values were also compared with the results obtained from the computational fluid dynamics (CFD) software and the experimental tests conducted in the setup.

## MATERIALS AND METHODS

Salt obtained from Izmir Salt Lake in Turkey was used in the drying experiment after undergoing pretreatment, which involved washing, grinding, and centrifugation. The salt was supplied in plastic containers by a company. It should be noted that salts typically have varying grain sizes. In this study, a moisture analyzer with an accuracy

of 0.01% (RADWAG brand, MA 50.X2.A model, Poland) was utilized.

In this study, the Reetsch brand AS 200 Basic model sieving device was used at 90 rpm for a duration of 10 min to sieve the salt product. Three replicate sieve analyses were performed to determine the size distribution of the particles of different diameters. The size distribution is a representation of the amount of product based on the particle diameter obtained from the sieve analysis. The analysis employed sieves with mesh sizes of 500, 1000, 2000, 3000, 3500, and 4000  $\mu\text{m}$ . After the sieving process was completed, the products collected on the sieves were weighed to determine the quantity of the product with that specific particle size. The size distribution of the sieve-analyzed product was determined by quantifying the amount of product based on the particle diameter. Once the sieving process was completed, the collected products on the sieves were weighed to determine the quantity of product for each particle size (Şengül et al. 2022). The mean diameters of the particles remaining in each sieve ( $D_{po}$ ) and the mean diameter by weight of the sieved material ( $D_{pas}$ ) were calculated using Equations 1 – 3.  $D_{pi}$  and  $D_{pi-1}$  represent the mesh sizes of two consecutive sieves (Pektaş 2022; Şengül 2022). CPR (cumulative percentage retained) and Fineness Modulus were calculated using Equations 4 and 5. To calculate the percentage retained (PR), the masses (individual/cumulative) for each sieve were divided by the total dry mass before washing. This result was then multiplied by 100 to determine the percentage of material that passed through and was retained by each sieve, as shown in Equation 6.

$$D_{p_{oi}} = \frac{(D_{pi} + D_{pi-1})}{2} \quad (1)$$

$$D_{pas} = \sum_{i=1}^n D_{p_{oi}} \cdot \Delta\Phi_i \quad (2)$$

$$\Delta\Phi_i = M_i / M_{tot} \quad (3)$$

$$CPR = \frac{CMR}{M} \times 100 \quad (4)$$

$$\text{Fineness Modulus} = \text{Cumulative percentage retained} / 100 \quad (5)$$

$$\text{PR} = (\text{Individual mass retained} / \text{Original dry mass of the sample}) \times 100 \quad (6)$$

where  $D_{pi}$  is the diameter of the largest particle in the sieve ( $\mu\text{m}$ ),  $D_{pi-1}$  is the diameter of the smallest particle in the sieve ( $\mu\text{m}$ ),  $\Delta\Phi_i$  is the material remaining on the sieve to the total sieved material rate,  $M_{tot}$  is the total amount of sieved material (g),  $M_i$  is the amount of material remaining on the sieve (g), CPR is cumulative percent

retained, CMR is cumulative mass retained, PR is percent retained, and M is total dry sample mass (g).

A laboratory-type static fluidized bed dryer belonging to the Asos Process Engineering Company was utilized in this study (Fig. 1). The air for drying purposes was heated using an electric heater, and the static fluidized bed dryer system was controlled through an operator panel. The desired air temperature during drying was recorded on the operator's screen.

In fluid bed dryers, the product slides across a perforated sheet with tiny holes, allowing air to come into contact with the product from all directions. It is assumed that the product's temperature and moisture at the dryer output are uniform throughout due to equal contact with the air.

The sieve plate serves as the surface on which the product is poured into the dryer, forming a bed through which the lower air passes to fluidize the product. Different sieve structures are available to suit product and dryer models. In the experiments, a mushroom-type sieve plate was used, designed specifically for optimal boiling and product advancement (Fig. 2). In continuous feeding machines, the airflow control is achieved by the sieve direction, which is the most effective method for product advancement.

Pressure loss occurs when the air pressurized by the fan equipment passes through the heater and duct. In addition, the sieve and product in the dryer create resistance to the compressed air. In this study, the



Fig. 1. Fluid bed dryer (1: Fan, 2: Resistance heater, 3: Hot air channel, 4: Dryer stand, 5: Product chamber, 6: Drying chamber, 7: Filter).



Fig. 2. Mushroom-type sieve plate.

counter-pressure value at which the sieve was created was called the under-sieve pressure, when the system was operated at the desired values without product feeding. Fig. 3 shows the manometer with which the under-sieve pressure value was measured.

In the trials, the salt product was placed on a sieve plate in the dryer feed chamber. Bed heights of 70, 80, and 90 mm were set (designated as *BH-1*, *BH-2*, and *BH-3*, respectively) and the effects of drying parameters were compared. Each trial lasted for 5 min. Salt samples were collected from the sampling section on the side of the drying chamber (Fig. 4a) and placed in airtight containers with a volume of 50 mL and a lid. Moisture levels were measured using a moisture analyzer (Pektaş 2022).

During the drying process, the fluidized powder products are carried away by the exhaust air. To prevent the escape of products and maintain dust control, a needle felt filter bag was attached to the dryer outlet (Fig. 4b). The filter bag captured the dust particles while allowing the exhaust air to pass through. Regular cleaning of the filter bags was performed during the trials.

In this study, the influence of air velocity (*AS*), bed height (*BH*), and drying air temperature (*DT*) on the drying process of salt products in a static fluidized bed dryer was investigated. The parameters used in the



Fig. 3. Sub-sieve pressure measurement manometer.

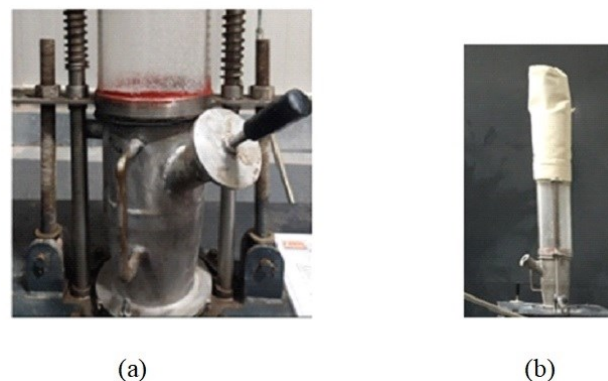


Fig. 4. (a) section for salt removal, (b) filter bag.

experiments are given in Table 1. The effects of these parameters on the moisture ratio and pressure drop were determined using theoretical calculations, CFD analysis, and laboratory experiments. The accuracy of the results obtained from these three different approaches was compared. The numerical values assigned to the parameters utilized in the experimental procedures are summarized in Table 2.

**Mathematical Modeling**

In the drying process, mathematical models are developed based on the characteristics of the input and desired final product. During dryer design, calculations such as minimum fluidization rate and pressure drop are crucial in determining the appropriate machine size for achieving the desired product capacity. This study employed the main formulations reported in the literature.

The Archimedean number (Ar) is calculated when two or more fluids with different densities are in motion. The Ar is determined based on the parameters specified in Equation 7 (Cocco et al. 2014). Equation 8 was used to compute the density (kg/m<sup>3</sup>) (Şengül et al. 2022).

$$Ar = [g \times p_p \times (p_p - p) \times d_p^3] / \mu^2 \quad (7)$$

$$p = 1.2 \times (293/T) \quad (8)$$

where g is the gravitational acceleration (m/s<sup>2</sup>), μ is the viscosity of air (kg/ms), p is the air density (kg/m<sup>3</sup>), p<sub>p</sub> is the sample density (kg/m<sup>3</sup>), d<sub>p</sub> is the sample diameter (m), and T is the drying air temperature (°C).

The minimum fluidization velocity, also known as the minimum surface velocity required to fluidize a bed, is

determined by the parameters described in Equation 9 (Ryu et al. 2003).

$$u_{mf} = \frac{\mu}{\rho_g \cdot d_p} \left( \frac{1,38 \times 10^{-3} \cdot Ar}{(Ar + 19)^{0,11}} \right) \quad (9)$$

In the fluidized bed dryer with a fixed bed type, there exists a porosity value that represents the air space between the particles. During fluidization, this porosity value changes due to the interaction between the air and particles (Naterer 2002). The porosity is calculated using Equation 10.

$$\epsilon = \epsilon_{mf} \cdot \left( \frac{Re_p + 0,02 \cdot Re_p^2}{Re_{mf} + 0,02 \cdot Re_{mf}^2} \right)^{0,21} \quad (10)$$

where ε denotes the bed void ratio (dimensionless).

As air passes through the fluidized bed, the air pressure decreases due to friction. The pressure drop is calculated using Equation 11 (Kurtuluş 2007), as follows:

$$\Delta P = h \cdot \rho_g \cdot U^2 \left[ \frac{150 \cdot (1 - \epsilon)}{Re_p \cdot \phi} + \frac{7}{4} \right] \frac{1 - \epsilon}{\phi \cdot d_p \cdot \epsilon^3} \quad (11)$$

where ε is bed void ratio (dimensionless), φ is sphericity (dimensionless), h is bed height (m), p<sub>g</sub> is density, Re is Reynolds number, and U is the velocity (m/s).

**Method of Analysis**

The Syamlal-O'Brien drag model, which characterizes the interaction between particles and air during turbulent fluidization, was used in this study. The dryer model utilized is depicted in Fig. 5. The bottom was defined as the air inlet, the top as the air outlet, and the side walls as non-slip surfaces. The dimensions of the dryer were 200

**Table 1. Research variables.**

Test No	Parameter-1	Parameter-1	Parameter-3	Test No	Parameter-1	Parameter-1	Parameter-3
1	AS -1	DT-1	BH-1	15	AS -2	DT-2	BH-3
2	AS -1	DT-1	BH-2	16	AS -2	DT-3	BH-1
3	AS -1	DT-1	BH-3	17	AS -2	DT-3	BH-2
4	AS -1	DT-2	BH-1	18	AS -2	DT-3	BH-3
5	AS -1	DT-2	BH-2	19	AS -3	DT-1	BH-1
6	AS -1	DT-2	BH-3	20	AS -3	DT-1	BH-2
7	AS -1	DT-3	BH-1	21	AS -3	DT-1	BH-3
8	AS -1	DT-3	BH-2	22	AS -3	DT-2	BH-1
9	AS -1	DT-3	BH-3	23	AS -3	DT-2	BH-2
10	AS -2	DT-1	BH-1	24	AS -3	DT-2	BH-3
11	AS -2	DT-1	BH-2	25	AS -3	DT-3	BH-1
12	AS -2	DT-1	BH-3	26	AS -3	DT-3	BH-2
13	AS -2	DT-2	BH-1	27	AS -3	DT-3	BH-3
14	AS -2	DT-2	BH-2				

**Table 2. Numerical values of parameters.**

Parameter-1	AS-1	AS-2	AS-3
Value	1.36 m/s	1.66 m/s	1.96 m/s
Parameter-2	DR-1	DR-2	DR-3
Value	120°C	140°C	160°C
Parameter-3	BH-1	BH-2	BH-3
Value	70 mm	80 mm	90 mm

mm × 1500 mm. In the analysis conducted in two dimensions, the bed height, air velocity, and air temperature were considered as independent variables.

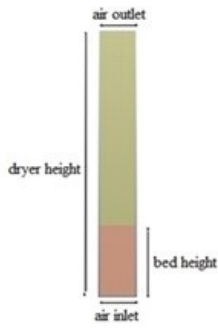


Fig. 5. Dryer model.

**Multiphase Flow with Interphase eXchanges (MFIx)**

Multiphase flows play a significant role in numerous operations within the power generation and chemical processing sectors. Computational Fluid Dynamics (CFD) serves as a valuable tool for the design and optimization of processes and reactors employed in these industries. The MFIx

suite of CFD software, which is an open-source and versatile multiphase CFD software, is well-suited for simulating the hydrodynamics, heat transfer, and chemical reactions across a broad range of flow conditions (Ansari et al. 2019).

**RESULTS AND DISCUSSION**

**Sieve Analysis Findings**

The results of the sieve analysis conducted on the salt used in the drying experiments are the average of three trials (Table 3). The theoretical calculations assumed a salt particle diameter of 2.4 mm. Moisture measurements of samples taken from three different regions within the

storage container were performed using a moisture analyzer, revealing an average moisture content of 3%.

**Pressure Drop Test Results**

As mentioned by Kepçeoğlu et al. (2020), random velocities were employed to ensure fluidization. During laboratory trials, the system was operated at air velocities of 1.36, 1.66, and 1.96 m/s without any product in the dryer. This allowed the pressure exerted by the sieve to reach the desired air velocity. In the test, sudden increases and fluctuations were observed on the manometer at the moment when the pressure created by the bed was overcome, leading to the transition to fluidization. For this study, it was assumed that the manometer value remained constant during fluidization. The manometer scale in existing laboratory-type static dryer systems typically ranges between 0 – 250 mbar. Since this range was wide within the scope of this study, the values were recorded based on observations. Consequently, there may be some deviations within acceptable limits for the obtained values. Table 4 presents the pressure values under the sieve and the manometer values measured during drying. The pressure drop caused by the product during drying tests was determined by subtracting the pressure under the sieve from the manometer value at the boiling moment.

Table 3. Salt sieve analysis results.

Sieve No	Mesh Opening (µm)	Mesh Number	Sample Mass (g)	Cumulative Mass Retained (g)	Percentage Retained %	Cumulative Retained %	Cumulative Percentage Retained
1	4000	5	33.40 ± 0.20	33.40	3.30	3.30	17 ± 0.50
2	3500	6	26.80 ± 0.30	60.20	2.60	6.00	30 ± 0.60
3	3000	8	24.40 ± 0.40	84.60	2.40	8.40	42 ± 0.30
4	2000	10	60.40 ± 0.30	145.00	6.00	14.50	73 ± 0.30
5	1000	20	43.40 ± 0.50	188.40	4.30	18.80	94 ± 0.80
6	500	30	11.00 ± 0.40	199.40	1.10	19.90	100 ± 0.40

Sample Quantity (g): 200  
 Number of Revolutions (r/min): 90  
 Test Time (min): 10  
 Fineness modulus = 456/100 = 4.56

Table 4. Pressure drop results from drying tests.

No	AS	DT	BH	US	PB	PP	No	AS	DT	BH	US	PB	PP
1	1.36	120	70	800.36 ± 0.60	1100.40 ± 0.50	300.08 ± 0.40	15	1.66	140	90	900.38 ± 0.40	1350.50 ± 0.60	450.40 ± 0.40
2	1.36	120	80	800.54 ± 0.20	1150.22 ± 0.40	350.18 ± 0.30	16	1.66	160	70	900.21 ± 0.60	1250.29 ± 0.50	350.24 ± 0.40
3	1.36	120	90	800.63 ± 0.40	1200.33 ± 0.50	400.56 ± 0.70	17	1.66	160	80	900.56 ± 0.70	1300.22 ± 0.70	400.23 ± 0.30
4	1.36	140	70	800.12 ± 0.20	1100.56 ± 0.30	300.44 ± 0.70	18	1.66	160	90	900.76 ± 0.40	1350.12 ± 0.70	450.34 ± 0.70
5	1.36	140	80	800.24 ± 0.90	1150.52 ± 0.80	350.66 ± 0.60	19	1.66	120	70	1000.65 ± 0.50	1400.03 ± 0.60	400.35 ± 0.80
6	1.36	140	90	800.48 ± 0.50	1200.55 ± 0.60	400.22 ± 0.50	20	1.96	120	80	1000.43 ± 0.50	1450.10 ± 0.80	450.45 ± 0.80
7	1.36	160	70	800.34 ± 0.50	1100.08 ± 0.70	300.20 ± 0.40	21	1.96	120	90	1000.32 ± 0.40	1500.13 ± 0.40	500.60 ± 0.60
8	1.36	160	80	800.51 ± 0.40	1150.66 ± 0.70	350.54 ± 0.40	22	1.96	140	70	1000.45 ± 0.30	1400.70 ± 0.50	400.44 ± 0.30
9	1.36	160	90	800.54 ± 0.60	1200.08 ± 0.80	400.10 ± 0.30	23	1.96	140	80	1000.43 ± 0.30	1450.21 ± 0.50	450.20 ± 0.50
10	1.66	120	70	900.10 ± 0.80	1250.50 ± 0.90	350.20 ± 0.50	24	1.96	140	90	1000.32 ± 0.10	1500.30 ± 0.40	500.21 ± 0.40
11	1.66	120	80	900.39 ± 0.40	1300.22 ± 0.50	400.33 ± 0.50	25	1.96	160	70	1000.51 ± 0.40	1400.20 ± 0.30	400.09 ± 0.40
12	1.66	120	90	900.45 ± 0.40	1350.49 ± 0.40	450.45 ± 0.60	26	1.96	160	80	1000.40 ± 0.30	1450.45 ± 0.60	450.02 ± 0.50
13	1.66	140	70	900.56 ± 0.60	1250.30 ± 0.50	350.53 ± 0.70	27	1.96	160	90	1000.21 ± 0.20	1500.55 ± 0.60	500.11 ± 0.30
14	1.66	140	80	900.58 ± 0.50	1300.54 ± 0.60	400.32 ± 0.30							

AS: Air Velocity (m/s). DT: Drying Air Temperature (°C). BH: Bed Height (mm). US: Under Sieve Pressure (Pa). PB: Pressure Value During Boiling (Pa). PP: Pressure Value Created by Product (Pa). Values for US, PB and PP represent the mean + SD of three replicate tests.

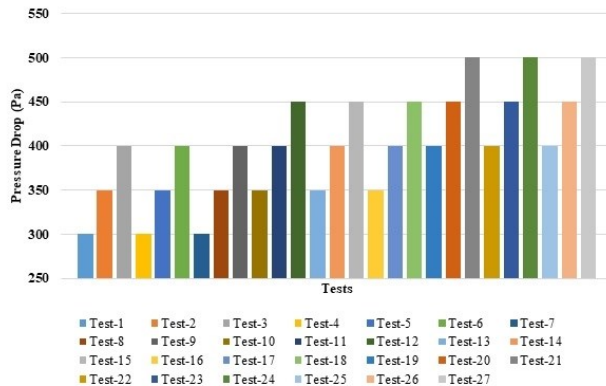


Fig. 6. The effect of the fluidized salt product on pressure drop.

The test plan and the pressure drop values created by the product are depicted in Fig. 6. Comparison of the tests revealed that the pressure drop increased with bed height and air velocity, while the temperature parameter had no observable effect on the pressure drop.

**Drying Results**

The duration of each test was 5 min, during which four samples were collected from the sampling chamber at intervals of 1.15 min. The moisture contents of these samples are listed in Table 5. The results indicate that the product achieved a moisture value considered dry, on average, after 3 min. To determine the parameter with the greatest impact on drying time, the moisture values of samples collected at 2.5 min were examined. The samples were collected using a fluidized bed.

As shown in Fig. 7, moisture removal from the product accelerated with increasing temperature and air velocity, but drying occurred later with an increase in bed height.

The upper body of the static dryer where the drying trials were conducted consisted of a glass pipe. Fig. 8

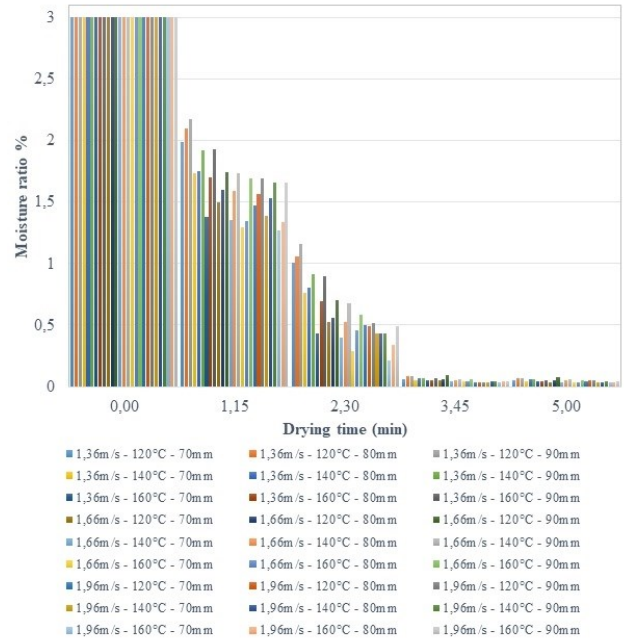


Fig. 7. Relationship between moisture ratio and drying time.

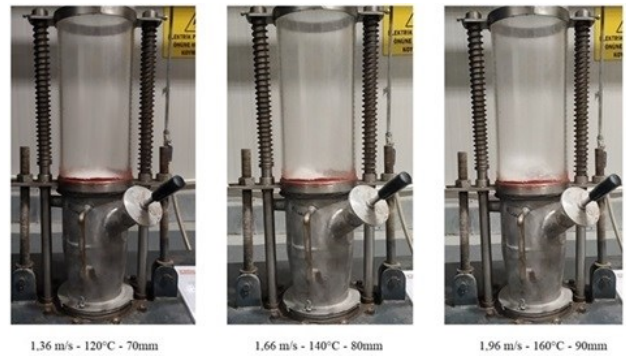


Fig. 8. Boiling images with various parameters.

shows the boiling movements observed in the glass region. It was observed that an increase in the parameters increased boiling action.

Table 5. Drying test moisture measurement results.

No	AS	DT	BH	IMV	FMV	SMV	TMV	OMV	No	AS	DT	BH	IMV	FMV	SMV	TMV	OMV
1	1.36	120	70	3	1.988	1.008	0.057	0.051	15	1.66	140	90	3	1.732	0.675	0.062	0.057
2	1.36	120	80	3	2.095	1.055	0.082	0.062	16	1.66	160	70	3	1.299	0.288	0.039	0.031
3	1.36	120	90	3	2.173	1.160	0.088	0.072	17	1.66	160	80	3	1.349	0.456	0.039	0.032
4	1.36	140	70	3	1.738	0.758	0.047	0.044	18	1.66	160	90	3	1.689	0.581	0.059	0.052
5	1.36	140	80	3	1.750	0.805	0.069	0.060	19	1.96	120	70	3	1.471	0.503	0.036	0.040
6	1.36	140	90	3	1.923	0.910	0.072	0.064	20	1.96	120	80	3	1.565	0.489	0.037	0.050
7	1.36	160	70	3	1.376	0.428	0.049	0.042	21	1.96	120	90	3	1.690	0.515	0.038	0.060
8	1.36	160	80	3	1.702	0.693	0.053	0.044	22	1.96	140	70	3	1.385	0.433	0.037	0.030
9	1.36	160	90	3	1.931	0.898	0.064	0.055	23	1.96	140	80	3	1.530	0.436	0.042	0.033
10	1.66	120	70	3	1.502	0.527	0.052	0.041	24	1.96	140	90	3	1.660	0.433	0.044	0.042
11	1.66	120	80	3	1.600	0.556	0.057	0.051	25	1.96	160	70	3	1.268	0.209	0.034	0.031
12	1.66	120	90	3	1.744	0.704	0.092	0.071	26	1.96	160	80	3	1.334	0.340	0.039	0.032
13	1.66	140	70	3	1.355	0.402	0.043	0.032	27	1.96	160	90	3	1.655	0.494	0.041	0.041
14	1.66	140	80	3	1.588	0.527	0.047	0.047									

IMV: Input Moisture Value, FMV: Moisture Value at 1<sup>st</sup> measurement, SMV: Moisture Value at 2<sup>nd</sup> measurement, TMV: Moisture Value at 3<sup>rd</sup> measurement.

Selecting the optimal boiling point for a product in a dryer system significantly impacts its design. If a velocity higher than necessary is chosen, the product may be carried away by the exhaust air, leading to its expulsion from the dryer. To minimize product loss, the dryer dome should have a large volume, and the piping should have large diameters to reduce exhaust velocity. Additional equipment is required to recover discarded products, which increases both the initial investment and maintenance costs.

**Mathematical Modeling Results**

The theoretically calculated parameters was presented in Table 6. The calculations were based on a particle diameter of 2.4 mm and a density of 1631 kg/m<sup>3</sup> for the salt product.

The pressure drop reached its highest value at a velocity of 1.96 m/s, which was the maximum velocity regardless of the temperature and bed height parameters (Fig. 9). This observation aligns with Kurtulus' (2007) findings, which indicated that an increase in the velocity parameter leads to an increase in pressure drop.

The graphical representation of the values obtained from the theoretical calculations are presented in Fig. 10. In contrast to velocity and bed height, the pressure drop decreased with an increase in temperature. This phenomenon can be attributed to the decrease in air

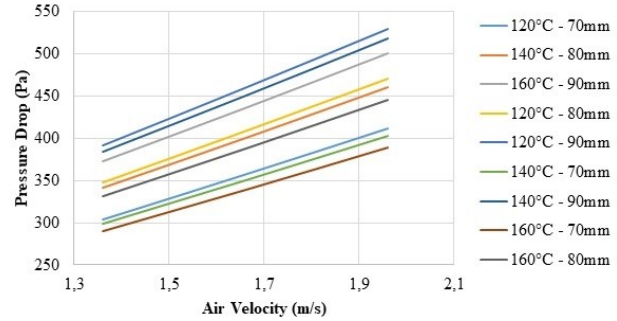


**Fig. 9. Effect graph of velocity parameter on pressure drop.**

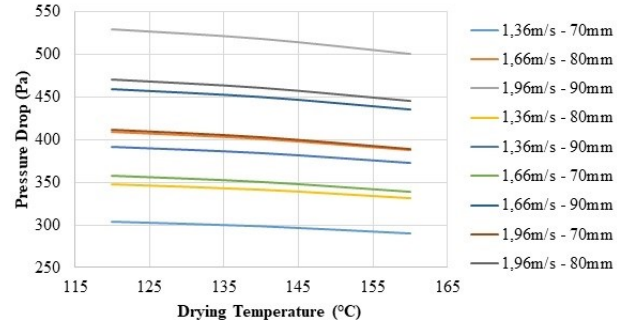


**Fig. 10. Effect of temperature parameter on pressure drop.**

density as the temperature rises. According to Equation 8, a decrease in air density leads to a decrease in pressure drop.

The increase in bed height led to an increase in pressure drop, as illustrated in Fig. 11, which is in line

**Table 6. Mathematical calculation results.**

No	AS	DT	BH	$\mu$	$\rho_g$	$\epsilon$	$Re_p$	Ar	$Re_{mf}$	$u_{mf}$	$\phi$	$\Delta P$
1	1.36	120	70	2.26E-05	0.899	0.610	130.02	3.90E+05	96.95	1.367	0.544	304.17
2	1.36	120	80	2.26E-05	0.899	0.610	130.02	3.90E+05	96.95	1.367	0.544	347.63
3	1.36	120	90	2.26E-05	0.899	0.610	130.02	3.90E+05	96.95	1.367	0.544	391.08
4	1.36	140	70	2.34E-05	0.869	0.609	121.40	3.50E+05	90.80	1.335	0.547	298.49
5	1.36	140	80	2.34E-05	0.869	0.609	121.40	3.50E+05	90.80	1.335	0.547	341.14
6	1.36	140	90	2.34E-05	0.869	0.609	121.40	3.50E+05	90.80	1.335	0.547	383.78
7	1.36	160	70	2.42E-05	0.818	0.606	110.43	3.00E+05	83.65	1.309	0.553	289.43
8	1.36	160	80	2.42E-05	0.818	0.606	110.43	3.00E+05	83.65	1.309	0.553	330.78
9	1.36	160	90	2.42E-05	0.818	0.606	110.43	3.00E+05	83.65	1.309	0.553	372.13
10	1.66	120	70	2.26E-05	0.899	0.657	158.70	3.90E+05	96.95	1.367	0.466	357.54
11	1.66	120	80	2.26E-05	0.899	0.657	158.70	3.90E+05	96.95	1.367	0.466	408.62
12	1.66	120	90	2.26E-05	0.899	0.657	158.70	3.90E+05	96.95	1.367	0.466	459.70
13	1.66	140	70	2.34E-05	0.869	0.655	148.18	3.50E+05	90.80	1.335	0.469	350.32
14	1.66	140	80	2.34E-05	0.869	0.655	148.18	3.50E+05	90.80	1.335	0.469	400.36
15	1.66	140	90	2.34E-05	0.869	0.655	148.18	3.50E+05	90.80	1.335	0.469	450.41
16	1.66	160	70	2.42E-05	0.818	0.651	134.79	3.00E+05	83.65	1.309	0.476	338.79
17	1.66	160	80	2.42E-05	0.818	0.651	134.79	3.00E+05	83.65	1.309	0.476	387.19
18	1.66	160	90	2.42E-05	0.818	0.651	134.79	3.00E+05	83.65	1.309	0.476	435.59
19	1.96	120	70	2.26E-05	0.899	0.699	187.38	3.90E+05	96.95	1.367	0.399	411.99
20	1.96	120	80	2.26E-05	0.899	0.699	187.38	3.90E+05	96.95	1.367	0.399	470.85
21	1.96	120	90	2.26E-05	0.899	0.699	187.38	3.90E+05	96.95	1.367	0.399	529.71
22	1.96	140	70	2.34E-05	0.869	0.696	174.96	3.50E+05	90.80	1.335	0.402	403.31
23	1.96	140	80	2.34E-05	0.869	0.696	174.96	3.50E+05	90.80	1.335	0.402	460.92
24	1.96	140	90	2.34E-05	0.869	0.696	174.96	3.50E+05	90.80	1.335	0.402	518.54
25	1.96	160	70	2.42E-05	0.818	0.692	159.15	3.00E+05	83.65	1.309	0.410	389.43
26	1.96	160	80	2.42E-05	0.818	0.692	159.15	3.00E+05	83.65	1.309	0.410	445.06
27	1.96	160	90	2.42E-05	0.818	0.692	159.15	3.00E+05	83.65	1.309	0.410	500.70

AS: Air Velocity (m/s). DT: Drying Air Temperature (°C). BH: Bed Height (mm).  $\mu$ : Viscosity of Air (kg/ms).  $\rho_g$ : Density of Sample (kg/m<sup>3</sup>).  $\epsilon$ : Bed Void Ratio (dimensionless).  $Re_p$ : Reynolds Number (dimensionless). Ar: Archimedeian Number (dimensionless).  $Re_{mf}$ : Reynolds Number at Minimum Fluidization Velocity (dimensionless).  $u_{mf}$ : Minimum Fluidization Velocity (m/s).  $\phi$ : Sphericity (dimensionless).  $\Delta P$ : Pressure Drop (Pa).

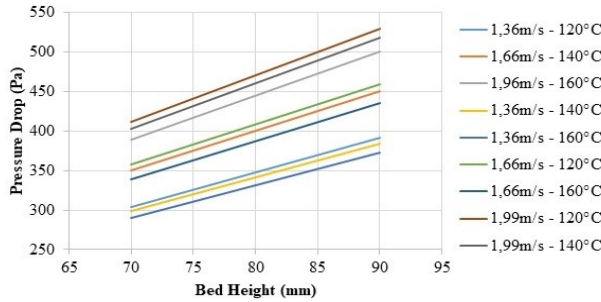


Fig. 11. Effect of bed height parameter on pressure drop.

with the findings reported by Kurtuluş (2007). The increased bed height creates greater resistance to the airflow, resulting in a higher pressure drop. Furthermore, it was observed that the pressure drop decreased with an increase in temperature at a constant bed height.

The high pressure drop observed at the beginning of the drying process is attributed to the high total mass of the product in the fluidized bed. As the drying air passes through the salt grains, flow resistance occurs, leading to the pressure drop. When the salts occupy a volume, the drying air attempts to pass through the spaces between them. With an increase in air velocity, the flow resistance also increases, resulting in an elevated pressure drop. Consequently, the pressure drop is dependent on the velocity of the drying air (Erçetin and Uralcan 2009; Parlak 2014; Ceylan and Gürel 2017).

Table 7. Comparison of the impact of the bed height parameter on pressure drop in MFIx analysis.

Test No	$\Delta P$
1	283.49
2	311.55
3	368.97
4	283.04
5	310.99
6	372.43
7	278.91
8	308.07
9	370.48
10	300.98
11	328.75
12	393.82
13	300.61
14	329.97
15	385.58
16	290.72
17	321.34
18	372.74
19	311.18
20	342.52
21	398.61
22	309.72
23	340.5
24	399.26
25	303.36
26	341.09
27	400.28

MFIx Analysis Results

The analysis aimed to investigate the effects of different parameters on boiling motion and pressure drop. The results of the analysis are presented in Table 7.

Fig. 12 displays boiling images captured at the 1.5<sup>th</sup> min for each analysis. Upon examining the boiling images, it became evident that an increase in air velocity aptly influenced the boiling motion.

The MFIx program's captured images in Fig. 13 reveal the visible effect of increasing air velocity on boiling. As the air velocity increased, fluidization increased, and the upward movement of the product increased. Boiling occurred when the air velocity was the lowest, such as in trials 1, 5, and 9, because the air velocity was higher than the minimum fluidization velocity. It can be observed that the boiling motion was more active at higher air velocities. In addition, it was concluded that temperature change did not have a visible effect on boiling.

The effect of the velocity parameter on the pressure drop is shown in Fig. 13, where the pressure drop increased with the velocity and bed height.

Temperature had a negative effect on the pressure drop (Fig. 14). Similar results are shown in Fig. 10.

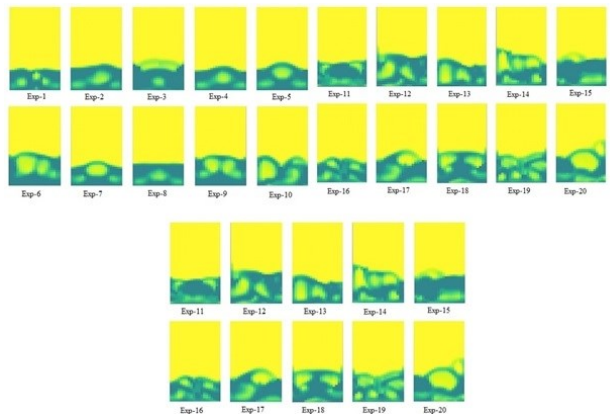


Fig. 12. MFIx analysis boiling images at 1.5<sup>th</sup> minute.

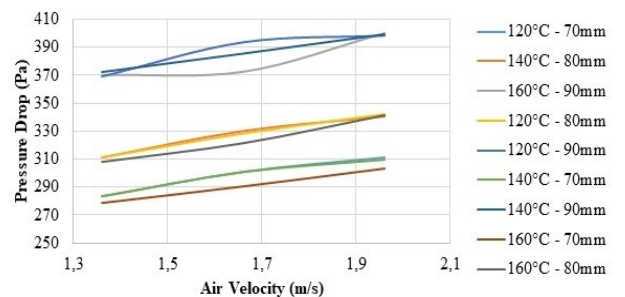


Fig. 13. Effect graph of velocity parameter on pressure drop.

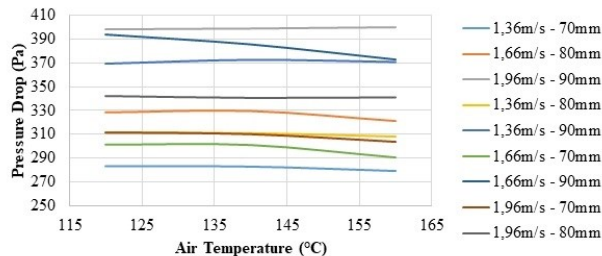


Fig. 14. Effect graph of temperature parameter on pressure drop.

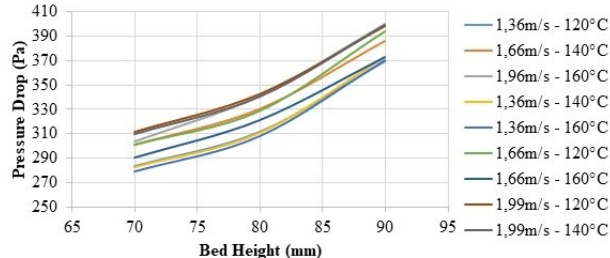


Fig. 15. Effect graph of bed height parameter on pressure drop.

Upon analyzing the pressure drop graph resulting from changes in velocity, it was observed that the pressure drop increased with higher air velocities, as predicted by the theoretical calculations. This pressure represented the average pressure drop when the system was in a static balance. The absence of a linear curve, as

seen in theoretical calculations, stemmed from variations in product movement across different analyses and time intervals. Piling up the product on one side at a particular moment caused a decrease in additional pressure on that side, preventing the graph from following a linear pattern. Furthermore, the increase in pressure drop with higher bed heights agreed with the theoretical calculations.

Pressure drop increased with an increasing bed height. Similar to the theoretical calculations, the graph did not exhibit a linear pattern but rather a parabolic one. This was due to the fact that, as mentioned in Fig. 15, the product tended to pile up towards one side during boiling, leading to an increase in pressure drop. Additionally, the analysis method determined that the bed height parameter had a more significant effect on pressure drop compared to other parameters.

This study employed three methods for calculating pressure drop: laboratory tests, mathematical methods, and analytical methods. Table 8 presents the consistency of the calculation methods. It was observed that an increase in the velocity and bed height parameters had the expected effect on the pressure drop, whereas an increase in the temperature parameter had an inverse effect. When comparing the impact of these parameters, it was found that air velocity had a more significant influence than bed height. Table 8 also shows no

Table 8. Comparison of pressure drop calculation methods.

No	AS	DT	BH	$\Delta P$		
				Experimental	Theoretical	MFIX
1	1.36	120	70	300	304.17	283.49
2	1.36	120	80	350	347.63	311.55
3	1.36	120	90	400	391.08	368.97
4	1.36	140	70	300	298.49	283.04
5	1.36	140	80	350	341.14	310.99
6	1.36	140	90	400	383.78	372.43
7	1.36	160	70	300	289.43	278.91
8	1.36	160	80	350	330.78	308.07
9	1.36	160	90	400	372.13	370.48
10	1.66	120	70	350	357.54	300.98
11	1.66	120	80	400	408.62	328.75
12	1.66	120	90	450	459.70	393.82
13	1.66	140	70	350	350.32	300.61
14	1.66	140	80	400	400.36	329.97
15	1.66	140	90	450	450.41	385.58
16	1.66	160	70	350	338.79	290.72
17	1.66	160	80	400	387.19	321.34
18	1.66	160	90	450	435.59	372.74
19	1.96	120	70	400	411.99	311.18
20	1.96	120	80	450	470.85	342.52
21	1.96	120	90	500	529.71	398.61
22	1.96	140	70	400	403.31	309.72
23	1.96	140	80	450	460.92	340.5
24	1.96	140	90	500	518.54	399.26
25	1.96	160	70	400	389.43	303.36
26	1.96	160	80	450	445.06	341.09
27	1.96	160	90	500	500.70	400.28

AS: Air Velocity (m/s). DT: Drying Air Temperature (°C). BH: Bed Height (mm).  $\Delta P$ : Pressure Drop (Pa). MFIX - Multiphase Flow with Interphase Exchanges.

statistically significant difference between the theoretical and experimental pressure drops ( $t$ -test for  $\Delta P_{\text{Theoretical}}$  and  $\Delta P_{\text{Experimental}}$ ,  $p > 0.05$ ). The difference between the pressure drops obtained from the MFIX analysis and experimental results was statistically significant ( $t$ -test for  $\Delta P_{\text{MFIX}}$  and  $\Delta P_{\text{Experimental}}$ ,  $p < 0.05$ ).

## CONCLUSION

One of the primary criteria for determining the velocity in a fluidized bed dryer is to ensure a minimum fluidization rate. For this purpose, calculations using the fluidization formula were done for the velocity parameter and for the velocity values at which fluidization would occur, namely 1.36, 1.66, and 1.96 m/s. Also, increasing the bed height resulted in a higher air velocity required for fluidization and a higher temperature necessary for drying. It was concluded that an increase in air velocity and bed height increased the pressure drop at the correct rate. When the theoretical calculations were analyzed, it was observed that the increase in air velocity had a greater effect on the pressure drop, whereas the bed height had a more significant impact overall. This disparity can be attributed to the accumulation of the product on one side during the boiling movement in the analysis and test environments. Moreover, an increase in temperature had an inverse effect on the pressure drop. This was due to a decrease in the density of the heated air. In the analysis method, it was observed that an increase in the temperature increased the pressure drop in some trials. This was attributed to the accumulation of the product during boiling. In conclusion, the most suitable values within the selected parameters for the laboratory-type static dryer system were determined to be 1.66 m/s for velocity, 160°C for temperature, and 70 mm for bed height.

## ACKNOWLEDGMENT

The authors would like to express their gratitude to Asos Process Engineering for granting the use of their laboratory facilities for this research.

## REFERENCES CITED

- ANSARI A, MOHAGHEGH SD, SHAHNAMEH M, DIETIKER JF. 2019. Modeling average pressure and volume fraction of a fluidized bed using data-driven smart proxy. *Fluids*. 4(3):123. doi:10.3390/fluids4030123.
- ASSARI MR, TABRIZI HB, SAFFAR-AVVAL M. 2007. Numerical simulation of fluid bed drying based on two-fluid model and experimental validation. *Appl Therm Eng*. 27(2–3):422–429. doi:10.1016/j.applthermaleng.2006.07.028.
- BAIT RG, PAWAR SB, BANERJEE AN, MUJUMDAR AS, THORAT BN. 2011. Mechanically agitated fluidized bed drying of cohesive particles at low air velocity. *Dry Technol*. 29(7):808–818. doi:10.1080/07373937.2010.541574.
- ÇALBAN T. 2006. The effects of bed height and initial moisture concentration on drying lignite in a batch fluidized bed. *Energy Source Part A*. 28(5):479–485. doi:10.1080/009083190928029.
- CEYLAN I, GÜREL AE. 2017. Akışkan yataklı kurutma sisteminin termodinamik analizi. Proceedings of the 1<sup>st</sup> International Conference on Energy Systems Engineering; 2–4 November 2017; Karabük, Turkey. (in Turkish)
- COCCO R, KARRI SR, KNOWLTON T. 2014. Introduction to fluidization. *Am I Chem Eng (AIChE)*. 110(11): 21–29. <https://www.aiche.org/sites/default/files/cep/20141121.pdf>.
- DEMİRKOL Ş, ÇİFÇİ İ, ÇİFÇİ H. 2018. The importance of rock salt in terms of gastronomy and faith: Hacibektaş rock salt. Proceedings of the 1<sup>st</sup> International Congress of New Generation and New Trends in Tourism; 01–03 November 2018; Sapanca, Turkey.
- ELIAS M, LARANJO M, AGULHEIRO-SANTOS AC, POTES ME. 2019. The role of salt on food and human health. In: Çinku MC, Karabulut S, editors. *Salt in the earth*. London: IntechOpen Press. p 19–45.
- ERÇETİN Ü, URALCAN İY. 2009. Experimental analysis of the drying of parboiled wheat in fluidized bed. *J ESOGU Eng Arc Fac*. 22(3):89–99. <https://dergipark.org.tr/en/download/article-file/320466>.
- ERSÖZ MA, DOĞAN H. 2010. Investigated by experimentally for drying lake salt in a fluid bed continuous dryer. *Pamukkale Univ J Eng Sci*. 16(2):155–163. [https://jag.journalagent.com/pajes/pdfs/PAJES\\_16\\_2\\_155\\_163.pdf](https://jag.journalagent.com/pajes/pdfs/PAJES_16_2_155_163.pdf).
- GODIN J, SANCHEZ F, PJONTEK D, BRIENS C, MCMILLAN J. 2023. Study of hydrodynamics and particle entrainment for a 0.6m diameter fluidized bed of a large group A powder. *Powder Technol*. 416:118179. doi:10.1016/j.powtec.2022.118179.
- GÜNGÖRMEZ H. 2015. In terms of economic activity: Tuzluca Kaya. *J Geogr*. 30:26–37. <https://dergipark.org.tr/tr/download/article-file/231261>.

- HAMZEHEI M. 2011. CFD modeling and simulation of hydrodynamics in a fluidized bed dryer with experimental validation. *Int Sch Res Notices*. 2011:131087. doi:10.5402/2011/131087.
- JAFARI H, FARAHBOD F. 2017. The experimental survey on the rotary dryer performance: drying of wetted salt from effluent bio wastewater. *J Appl Biotechnol Bioeng*. 4(3):567–570. doi:10.15406/jabb.2017.04.00101.
- JALALI P, NIKKU M, RITVANEN J, HYPPANEN T. 2018. Flow characteristics of circulating fluidized beds near terminal velocity: Eulerian model of a lab-scale apparatus. *Powder Technol*. 339:569–584. doi:10.1016/j.powtec.2018.08.046.
- KAMBLE LV, PANGAVHANE DR, SINGH TP. 2014. Experimental investigation of horizontal tube immersed in gas-solid fluidized bed of large particles using artificial neural network. *Int J Heat Mass Transf*. 70:719–724. doi:10.1016/j.ijheatmasstransfer.2013.11.073.
- KEPCEOĞLU S, MORALAR A, ÇELEN S. 2020. determination of the ideal flow rate in drying of table salt. In: Kalkancı M, editor. *Theory and research in engineering II*. Ankara, Turkey: Gece Publishing. p. 35–46.
- KURTULUŞ O. 2007. Akışkan yatakta kurutma prosesinin incelenmesi. [master's thesis]. İstanbul, Turkey: Yıldız Technical University.
- MAHMOODI B, HOSSEINI SH, AHMADI G. 2019. CFD-DEM simulation of a pseudo-two-dimensional spouted bed comprising coarse particles. *Particuology*. 43:171–180. doi:10.1016/j.partic.2017.12.014.
- MORALAR A, ÇELEN S. 2022. Evaluation of thermal and drying characteristics of dried hazelnut (*Corylus avellana* L.) shell waste. *Philipp Agric Scientist*. 105(2):159–168. <https://pas.cafs.uplb.edu.ph/journal-issues/evaluation-of-thermal-and-drying-characteristics-of-dried-hazelnut-corylus-avellana-l-shell-waste/>.
- NATERER GF. 2002. *Heat transfer in single and multiphase systems*. Boca Raton (FL): CRC Press. 640 p. ISBN:9780367395865.
- PARLAK N. 2014. Investigation of drying kinetics of ginger in a fluidized bed dryer. *J Fac Eng Archit Gaz*. 29(2):261–269. <https://hdl.handle.net/20.500.12619/49869>.
- PEKTAŞ S. 2022. An optimization of factors affecting the performance of fluidized bed dryer. [master's thesis]. Tekirdag, Turkey: Namik Kemal University.
- RYU HJ, LIM NY, BAE DH, JIN GT. 2003. Minimum fluidization velocity and transition velocity to fast fluidization of oxygen carrier particle for chemical-looping combustor. *Hwahak Konghak*. 41(5):624–631. [https://www.researchgate.net/publication/228453735\\_Minimum\\_Fluidization\\_Velocity\\_and\\_Transition\\_Velocity\\_to\\_Fast\\_Fluidization\\_of\\_Oxygen\\_Carrier\\_Particle\\_for\\_Chemical-Looping\\_Combustor](https://www.researchgate.net/publication/228453735_Minimum_Fluidization_Velocity_and_Transition_Velocity_to_Fast_Fluidization_of_Oxygen_Carrier_Particle_for_Chemical-Looping_Combustor).
- ŞENGÜL A. 2022. Analysis of drying process of silica sand in vertical type fluid bed dryer. [master's thesis]. Tekirdag, Turkey: Namik Kemal University.
- ŞENGÜL A, ÇELEN S, HAKSEVER A. 2022. Investigation of the temperature change of sand dried at different temperatures in a pilot type fluidized bed dryer. In: Bellitürk S, Solmaz Y, editors. *Agricultural practices and sustainable management in Türkiye*. Ankara, Turkey: Iksad Publishing House. p. 51–70.